Review of Scientific Instruments ARTICLE pubs.aip.org/aip/rsi

High voltage determination and stabilization for collinear laser spectroscopy applications

Cite as: Rev. Sci. Instrum. 95, 083307 (2024); doi: 10.1063/5.0218649
Submitted: 13 May 2024 • Accepted: 6 August 2024 •
Published Online: 23 August 2024

Kristian König,[1,2,a] Finn Köhler,[1] Julian Palmes,[1] Henrik Badura,[3] Adam Dockery,[2,4] Kei Minamisono,[2,4] Johann Meisner,[3] Patrick Müller,[1] Wilfried Nörtershäuser,[1,5] and Stephan Passon[3]

AFFILIATIONS

[1] Institut für Kernphysik, Department of Physics, Technische Universität Darmstadt, 64289 Darmstadt, Germany
[2] Facility for Rare Isotope Beams, Michigan State University, East Lansing, Michigan 48824, USA
[3] Physikalisch-Technische Bundesanstalt, 38116 Braunschweig, Germany
[4] Department of Physics and Astronomy, Michigan State University, East Lansing, Michigan 48824, USA
[5] Helmholtz Forschungsakademie Hessen für FAIR (HFHF), Campus Darmstadt, Schlossgartenstr. 9, 64289 Darmstadt, Germany

[a] **Author to whom correspondence should be addressed:** kkoenig@ikp.tu-darmstadt.de

ABSTRACT

Fast beam collinear laser spectroscopy is the established method to investigate nuclear ground state properties such as the spin, the electromagnetic moments, and the charge radius of exotic nuclei. These are extracted with high precision from atomic observables, i.e., the hyperfine splitting and the isotope shift, which become possible due to a large reduction of the Doppler broadening by compressing the velocity width of the ion beam through electrostatic acceleration. With the advancement of experimental methods and applied devices, e.g., to measure and stabilize the laser frequency, the acceleration potential became the dominant systematic uncertainty contribution. To overcome this, we present a custom-built high-voltage divider, which was developed and tested at the German metrology institute, and a feedback loop that enabled collinear laser spectroscopy to be performed at a 100-kHz level. Furthermore, we describe the impact of field penetration into the laser–ion interaction region. This affects the determined isotope shifts and hyperfine splittings if Doppler tuning is applied, i.e., the ion beam energy is altered instead of scanning the laser frequency. Using different laser frequencies that were referenced to a frequency comb, the field penetration was extracted laser spectroscopically. This allowed us to define an effective scanning potential to still apply the faster and easier Doppler tuning without introducing systematic deviations.

I. INTRODUCTION

Long-term stable high-voltage sources are key for a variety of modern high-precision experiments: in particle physics, e.g., for the determination of the neutrino mass by measuring the beta-decay electron-end point energy[1,2] or for the operation of large-scale calorimeters;[3] in nuclear physics, e.g., for the determination of masses[4–6] or charge radii;[7] in atomic physics, e.g., in storage ring experiments;[8,9] and in the search for physics beyond the standard model by measuring the atomic electric dipole moment.[10] Although those fields and their experimental approaches are diverse, they depend on stable high voltages to apply accurate electric fields, accelerate charged particles, or define trap potentials. In this work, we focus on the application of collinear laser spectroscopy, which probes electrons in the atomic shell. This technique enables the measurement of exotic systems such as highly charged particles to test quantum electrodynamics (QED) in extreme fields[8,11] or to investigate the nuclear ground state properties of short-lived isotopes.[12,13] Thanks to the advances in laser frequency measurements, a relative accuracy of 10^{-9} can be easily achieved with modern wavelength meters or frequency combs, which is sufficient for these applications.[14,15] At the present time, the systematic limitation of this experimental approach is the measurement of the beam energy and, hence, the precise determination of the electrostatic acceleration potential. Since field penetrations, space-charge effects, and contact voltages, which can hardly be quantified, add to the applied acceleration potential, the kinetic beam energy can be determined most precisely by calibration measurements with reference

isotopes.[16] However, long-term measurements strongly rely on stable conditions and are mostly limited by drifting high voltages. In this work, we present our approach to measure these voltages and apply a stabilization scheme to reduce drifts to a 1-part-per-million (ppm) level. Similar approaches, which have been developed for different high-precision physics experiments, are described in Refs. 17–21. Furthermore, we present a procedure to quantify field penetration into the laser–ion interaction region since this critically affects the commonly applied voltage scans, which match the resonance condition between Doppler-shifted laser frequency and atomic transition.

II. SETUP

In collinear laser spectroscopy experiments, an ion beam with a kinetic energy of a few 10 keV is used, which has been electrostatically accelerated by floating the ion source on a high-voltage potential. The ion beam is then superposed with a laser beam, and by scanning the laser frequency in the rest-frame of the ion, an electronic transition is probed. At resonance, the ions are excited and emit fluorescence light that can be detected with photo-multiplier tubes. Due to the Doppler effect, the resonance frequency ν_0 in the rest-frame of the ion differs from the laser frequency ν_{lab} measured in the laboratory frame according to

$$\nu_0 = \nu_{\mathrm{lab}}\gamma(1 - \beta\cos(\alpha)), \tag{1}$$

with the time-dilation factor $\gamma = (1-\beta^2)^{-1/2}$, the velocity β in units of the speed of light and the angle α between ion and laser beam, which is $\alpha = 0^\circ$ for collinear and $\alpha = 180^\circ$ for anticollinear geometry. To extract the rest-frame transition frequency, the kinetic energy and, hence, the acceleration potential need to be precisely known. This is challenging due to the large uncertainties of the starting potential at the ion source, contact voltages, and contributions caused by field penetration into the laser–ion interaction region. Luckily, in relative measurements for the determination of differential charge radii from isotope shifts or electromagnetic moments from the hyperfine splitting, the demands on the knowledge of the absolute beam energy are largely reduced to a few eV, with the exception of the lightest elements.[7,22,23] However, potential changes during these relative measurements are critical, and drifts of the acceleration voltage of ≈100 mV exceed the typical uncertainty, even for heavier isotopes.

Precision measurements of the rest-frame transition frequency ν_0 can, nevertheless, be performed by probing the ion beam in collinear (↑↑) and anticollinear (↑↓) geometry,

$$\nu_0 = \sqrt{\nu_{\mathrm{lab},\uparrow\downarrow}\cdot\nu_{\mathrm{lab},\uparrow\uparrow}}, \tag{2}$$

to become independent of the kinetic energy.[23–25] Again, drifts of the beam energy between the alternately performed collinear and anticollinear measurements need to be suppressed to avoid systematic deviations. Having extracted ν_0 once, it can be used in turn to deduce the kinetic beam energy E_{kin} from a single measurement in collinear or anticollinear geometry,

$$E_{\mathrm{kin}} = \frac{mc^2}{2}\frac{(\nu_0 - \nu_{\mathrm{lab}})^2}{\nu_0\nu_{\mathrm{lab}}}. \tag{3}$$

This allows one to determine the offset between acceleration voltage and kinetic beam energy and reduces the corresponding uncertainty significantly.[16] Such a beam-energy determination via the Doppler-shift method has also been applied previously to accurately measure high voltages.[26,27]

Faster and technically easier than scanning the laser frequency ν_{lab} is altering the ion velocity by applying a scan voltage to the laser–ion interaction region. Since the laser frequency in the rest frame of an ion is then altered by changing the Doppler shift depending on the applied scan voltage, this procedure is called Doppler tuning. For a single resonance peak, the typical scan range is <50 V, and the systematic impact, e.g., due to field penetration, on the rest-frame frequency [Eq. (2)] or the isotope shift is small as long as the measurements of the targeted isotopes and the reference isotope are performed at approximately the same scan voltage. This, however, requires the laser frequency to be changed between the measurements of different isotopes. Keeping the laser frequency constant for different isotopes or investigating isotopes with large hyperfine splitting requires applying scan voltages between 100 V and a few kV. Field penetration into the interaction region depends on its geometry but can significantly impact the observed shift of the transition lines if present.

All measurements discussed in this work were performed at the collinear laser spectroscopy facilities at Michigan State University (MSU) and TU Darmstadt (TUDa). For a detailed description of the respective setups, we refer to Refs. 28 and 29. Here, we restrict the description to dedicated details of the recently installed high-voltage stabilization schemes.

A. MSU setup

At the BEam COoler and LAser spectroscopy (BECOLA) facility at MSU, ion beams are available from the Facility for Rare Isotope Beams or from a local offline Penning ion source. The ions are first fed into a He-buffer-gas-filled radio frequency quadrupole trap (RFQ) for beam cooling and bunching before collinear laser spectroscopy is performed. The offline source as well as the RFQ, including respective electronic devices, are floated with a FUG HCP 350–65 000 MOD on 30 kV. This voltage is measured with a high-voltage divider and a digital voltmeter (Keysight 34465A). The former commercial Ohmlabs HVS series divider was replaced by a new custom-made high-voltage divider described below, and the measured voltage was used as the input parameter of a feedback loop to stabilize the total high voltage. The FUG power supply enables the ground of the voltage generator to be separated from the common ground and, hence, allows us to apply a small correction voltage to float the FUG and stabilize its total output voltage, as shown in Fig. 1(a). The observed drifts of up to 2 V per day were compensated with a small correction voltage generated with a LabJack T4 digital-to-analog converter (DAC), while the FUG power supply is always kept at the same setpoint. With the 0–5 V DAC output of the LabJack, a resolution $<10^{-7}$ of the total voltage is achieved, which is not possible when regulating the power supply itself as all of the applied high-voltage power supplies offer a resolution at the 10^{-5} level. Finally, the long-term stability of the MSU setup is limited by the stability of the applied 6.5-digit multimeter, which has a specified drift of less than 13 ppm/day. Comparing three of these devices by measuring a test voltage, much smaller drifts were observed. Hence,

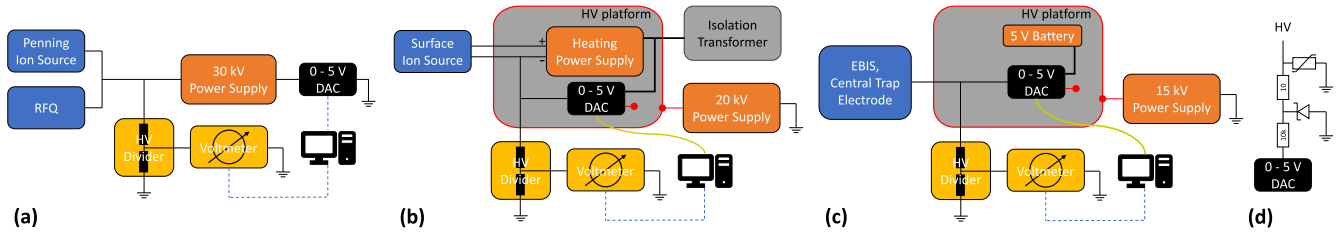

FIG. 1. Voltage stabilization schemes at (a) MSU and (b) and (c) TUDa in combination with different ion sources. The ion sources (shown in blue) are supplied with the acceleration voltage via a high-voltage cable and are connected to the ion beamline through ceramic high-voltage breaks. In all approaches, the total voltage applied to the ion source is measured with a custom-made voltage divider and a digital voltmeter. A feedback loop corrects the high voltage with a 0–5 V DAC unit using a simple proportional correction with an update time of 1 s, which is the integration time of the digital voltmeters. At MSU (a), the high-voltage power supply can be floated on this correction voltage, which is impossible with the device used at TUDa. Here, (b) and (c), the DAC unit is placed on a high-voltage platform. Electrical connections to the platform are shown in red. Communication with the DAC is realized via optical fiber (yellow). Using the surface ionization source (b) also requires a power supply that generates the heating current on the high-voltage platform, which is supplied with line voltage using an isolation transformer. The operation of the EBIS (c) does not require additional devices, and the DAC can be supplied from a 5-V battery, which removes the voltage noise induced by the isolation transformer. To avoid malfunctions caused by high-voltage sparks, the DAC is protected with a varistor and a transient-voltage suppressor diode (d) in all cases.

its drift during a typical measurement (up to 4 h) was concluded to be at the ppm level.

B. TUDa setup

At COALA (TU Darmstadt), different high-voltage power supplies are used for the surface ionization source (SIS) and electron beam ion source (EBIS). In both cases, the voltage generator cannot be separated from the common ground of the device, inhibiting direct floating by the correction voltage. Instead, the DAC unit to apply the correction voltage is placed on the high-voltage platform of the ion source.

In Fig. 1(b), the setup of the SIS is shown, which is used to produce beams of elements with low ionization potentials, such as alkaline and earth alkaline metals or lanthanides, by directly heating a graphite crucible. The high voltage of up to 20 kV is generated with a Heinzinger PNChp 20 000–10pos that was measured to drift with up to 40 mV/20 min, which corresponds to the time needed for a typical measurement. The voltage is applied to a high-voltage platform, housing the heating power supply and the DAC unit, and measured with a high-voltage divider and a Keysight 3458A 8.5-digit multimeter. The ion-source voltage is corrected by connecting the DAC to the negative pole of the heating power. This eliminates the drifts and reduces the short-term voltage variations to 10mV in the range of seconds.[30] At even shorter timescales, a 50-Hz power line hum with amplitudes <0.5 V is introduced by the isolation transformer. As laser-spectroscopy measurements average over many of these cycles, this introduces a broadening of the line shape. Due to the Doppler compression, however, the observed spectral width is still at the level of the natural linewidth. The DAC is controlled via fiber from the measurement PC.

The EBIS at COALA is operated in continuous mode, as this yields superior beam properties compared to pulsed operation.[31] In this mode, the ions are produced in a trap with three electrodes at fixed potentials supplied by ISEG HM81001 power supplies that were measured to drift up to 100 mV/20 min. For measurements in light, highly charged ions, as e.g., reported in Refs. 31 and 32 for $^{12}C^{4+}$, the central electrode that mainly determines the beam energy is stabilized by placing the DAC unit on a high-voltage platform and feeding the correction voltage to the electrode, as depicted in Fig. 1(c). To avoid the additional noise that is generally introduced when using an isolation transformer, the DAC unit was supplied with batteries. In the future, this system will be expanded to also control the end-cap electrode through which the beam leaves the source.

In the TUDa configuration with the DAC on the high-voltage platform, the commercial DAC unit endured only a few high-voltage sparks that occasionally occurred when operating the ion sources at their limits. A custom solution was designed, which is based on a 12-bit MCO4728 DAC with four channels. Matched to our capacity and high voltage, the first guard is an AMLV22 varistor combined with a 10 Ω resistor. Residual currents are deflected through a SMBJ5.0A transient voltage suppressor (TVS) that shields the DAC together with a 10 kΩ resistor, as depicted in Fig. 1(d). In addition, the power supply line of the DAC is connected to the identical guard setup. So far, the DAC, supplied with such shielding, has required not any replacements. Furthermore, a serial-to-fiber connection was integrated into the custom-built board, which allows direct communication with the PC on the ground potential.

C. High-voltage divider setup

The high-voltage dividers used at MSU and TUDa are custom made and based on the identical design[33] and only differ in the divider ratio of 3000:1 and 2000:1, respectively, to scale the maximum applied voltage of 30 and 20 kV to 10 V in both cases. To match the requirement of a high temporal stability of the divider ratio, the dividers consist of a chain of resistors with a low-temperature coefficient of <1 ppm/K. This is achieved with Caddock film resistors of type USF370 with a resistance of 9.95 MΩ each that were individually characterized by the manufacturer and selected in sets of five to achieve a minimal total temperature coefficient. The maximum operation voltage is 1 kV/resistor, leading to a total resistance of 298.5 and 199 MΩ, respectively. As the low voltage resistor, a Vishay foil resistor Y0007100K000 T9L (100 kΩ, <2 ppm/K) is used. All resistors are placed inside a ±0.1 K temperature-stabilized housing to be independent of the ambient conditions. The resistor chain winds in a helix structure around a cylinder. This tower

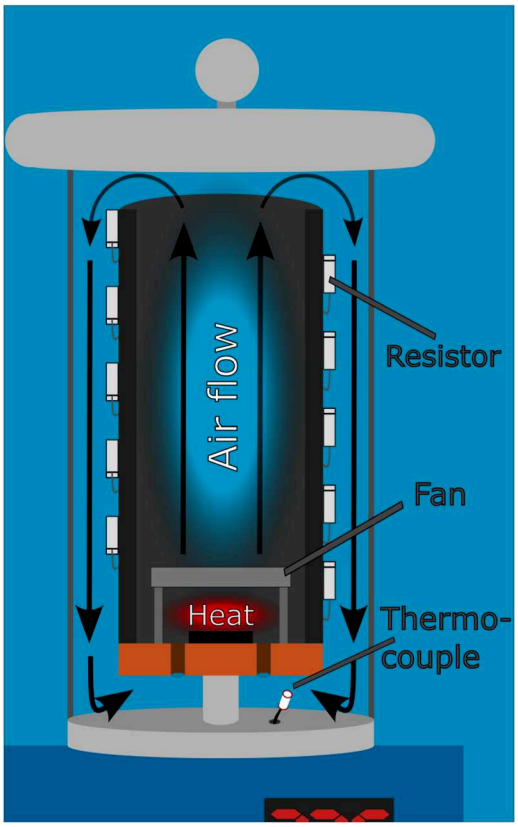

FIG. 2. Cross section of the high voltage divider, illustrating the air flow in the temperature stabilized housing. The temperature of the returning air is measured with a thermocouple element. With an Omron E5CN-HV2M-500 temperature controller, the heating current is adapted to stabilize the temperature to 30.0 °C.

is surrounded by an acrylic glass tube and closed by metallic lids on the top and bottom. The basic principle of temperature stabilization is shown in Fig. 2. A thick copper plate in the center is heated to 30.0(1)°C, and a ventilator creates a constant airflow that pushes up in the center and down on the outside, where the resistors are mounted. The heat created by the heater and the resistors is, therefore, equally distributed in the volume of the housing. As the temperature of the divider is set to a value above room temperature, there is passive cooling by the heat loss through the housing. The high voltage is applied to the top lid of the housing, which has a toroidal shape to avoid discharges. The low-voltage end is at the bottom, which is on ground potential. The electronics for the temperature stabilization are placed in a metallic box below, which also serves as the stand for the divider.

III. MEASUREMENTS

A. Calibration of the high-voltage divider

To characterize a high-voltage divider and calibrate its scale factor, it has to be compared to a reference divider. At both facilities, this was done with the same reference divider, MT100, from PTB, which is used as the national metrology standard for DC high

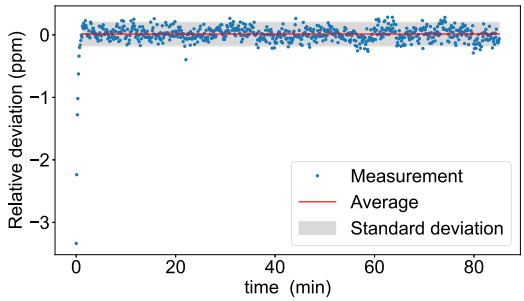

FIG. 3. Relative deviation of the TUDa divider scale factor over time measured against the MT100 reference from PTB.

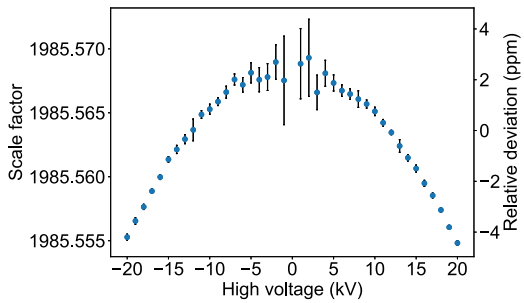

FIG. 4. Scale factor of the TUDa divider for different high voltages measured with the MT100 reference from PTB.

voltages.[34] As an example, we detail the calibration of the TUDa divider. The high voltage of interest is applied to both dividers, and the voltage is recorded with two Keysight 3458A multimeters. This measurement is performed for several voltages and also for a short-circuited divider to determine the contact voltages of the cables. The gain of the multimeters was calibrated with a Fluke 732C 10-V reference. In addition, the cable offset was considered.

First, the long-term stability of the scale factor was investigated by applying the maximum high voltage to the custom divider and the MT100 reference divider. The relative deviation of the scale factor over time is shown in Fig. 3. After about 1 min, the scale factor reached an equilibrium value that stayed constant over the whole measurement time of >80 min. The standard deviation indicated in Fig. 3 is about 0.2 ppm, which is well below the stabilization goal of <1 ppm.

As depicted in Fig. 4, the voltage dependence of the scale factor of the TUDa divider was determined in steps of 1 kV up to the maximum voltage of 20 kV. At each step, the measurement time was sufficiently long to reach thermal equilibrium. Repeating this process for both polarities leads to a parabolic shape of the data points. This is directly connected to the ohmic losses inside the divider. As the power of the losses $P_\Omega = U^2/R$ is directly proportional to the square of the voltage applied to the divider, the equilibrium temperature of the resistors is equally affected, which alters the resistance according to the temperature coefficient.

The total uncertainty of the calibration of the scale factor at PTB is composed of the statistical uncertainty in Fig. 4 and the uncertainty of the reference divider MT100 of about 2 ppm (2–σ range; all

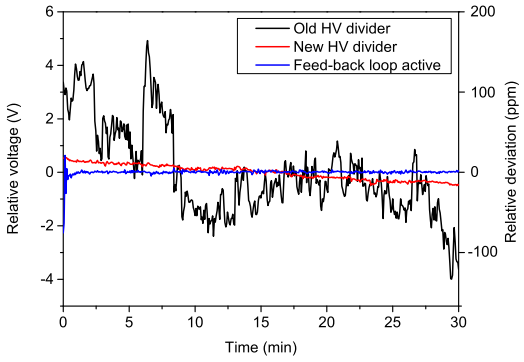

FIG. 5. 30-kV high-voltage measurement at BECOLA using a commercial high-voltage divider (black) and the present custom built divider (red) read out by 6.5 digit digital voltmeters. While the present divider showed a realistic slow drift of the high voltage, the commercial divider caused significant fluctuations in the voltage reading. Using the present divider and a feedback loop, the slow, most-likely thermal drift of the power supply was compensated.

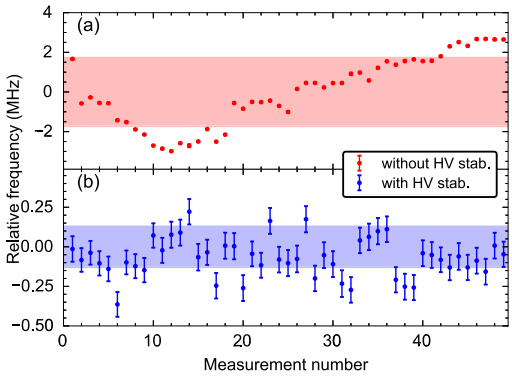

FIG. 6. Stability of the $5s\ ^2S_{1/2} \rightarrow 5p\ ^2P_{1/2}$ resonance frequency measurement in $^{88}Sr^+$ with and without active high-voltage stabilization of the ions' starting potential. Particularly in the first hour after starting the power supply, the output voltage slowly settles, which was the case in (a). Due to the Doppler effect, the determined frequency changes with the starting potential and, hence, the ion velocity drift. This can be circumvented when using active high-voltage stabilization, as shown in (b), which was also measured in the first hour after starting the power supply. The shaded area corresponds to the standard deviation and decreases from 1.7 MHz to 130 kHz if the voltage-stabilization is active. The error bars in (a) and (b) depict the statistical uncertainty, which is similar for all measurements.

other uncertainties are given as a $1-\sigma$ range). In addition, long-term drifts, i.e., due to the aging of the resistors, need to be considered, which can change the scale factor by several ppm per year.[33] Hence, this calibration process needs to be repeated regularly.

B. HV stability at MSU

At MSU, a high-voltage divider was built as described above to replace the former commercial Ohmlabs HVS series divider. Initially, the Ohmlabs divider performed well but then started to yield unrealistic readings. In Fig. 5, the voltage applied with the ultra-stable FUG was measured with both dividers. While the new custom-built divider shows a small and steady drift of the high-voltage, which is commonly observed as power supplies tend to drift for hours after start to reach thermal equilibrium, the voltage measured with the old Ohmlabs divider shows unrealistic drifts and jumps. Using laser spectroscopy to quantify the voltage stability as described in Sec. III C also revealed that these large drifts are not real but rather an artifact of the divider's measurement. To eliminate the long-term drift of the high voltage, the stabilization scheme described in Sec. II A was applied. The resulting voltage shows high stability after an initial overshooting of the feedback loop, as depicted in Fig. 5.

C. HV stability at TUDa

At TU Darmstadt, a similar feedback loop is employed to stabilize the high-voltage applied to the ion sources. In addition to the electronic measurement, collinear laser spectroscopy of the $5s\ ^2S_{1/2} \rightarrow 5p\ ^2P_{1/2}$ transitions in $^{88}Sr^+$, produced in the surface ionization source, was employed to probe the high-voltage stability. For this purpose, 50 measurements at 20 kV in anticollinear geometry were performed over a time period of 4 h. Any voltage drift causes a change in the determined resonant laser frequency due to different Doppler shifts, according to Eq. (1). In Fig. 6, the observed transition frequencies are plotted for the cases without (top) and with (bottom) voltage stabilization. In these measurements, Doppler tuning was applied, as described above, and the laser frequency was locked to a reference cavity that was long-term stabilized to a frequency comb, achieving a frequency stability of <100 kHz at the relevant timescale, which is limited by the linewidth of the employed laser system.[29] As shown in Fig. 6, the voltage stabilization significantly improved the reproducibility and reduced the standard deviation of the determined resonance frequencies from 1.7 MHz to 130 kHz. This is crucial to reach the highest precision of rest-frame frequencies from collinear–anticollinear measurements and isotope shifts, e.g., to test an atomic theory[30] or to search for nonlinearities in a King-plot.[35]

IV. FIELD PENETRATION INTO THE INTERACTION REGION

Applying Doppler tuning to scan across the resonance condition can require large scan voltages of 100 V to several kV if a large isotope shift or hyperfine splitting has to be covered. As the laser–ion interaction region, to which the high voltage is applied, requires openings for the ion and laser beams and the fluorescence detection, field penetration from the surrounding beamline components at ground potential can affect the potential experienced by the ion beam. In first order, field penetration affects the measured hyperfine splitting or isotope shift linearly and shifts it to smaller absolute values and, hence, can be corrected in the data analysis if the effect is well quantified. Therefore, the setups at MSU and TUDa were mapped accordingly.

For the characterization of the fluorescence detection region (FDR) at TUDa, which is depicted in Fig. 7 and contains two separate detection chambers, a single peak of the hyperfine spectrum of the $4f^{13}6s \rightarrow 4f^{13}6p$ transition at 384.0 nm in $^{169}Tm^+$ was used. First, collinear and anticollinear measurements were performed to extract its rest-frame frequency ν_0 with Eq. (2). The laser frequencies were adjusted for the resonances to appear at the same scan voltage.

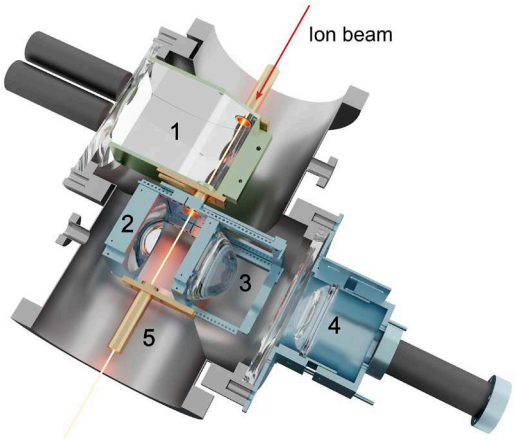

FIG. 7. Fluorescence detection region (FDR) of COALA at TUDa. In the first segment, an elliptical mirror (1) focuses fluorescence emitted from the beam axis onto two PMTs. In the second segment, a mirror (2) and two lenses (3) and (4) focus fluorescence light emitted from their focal points onto a single PMT. Small tubes (5) define the electrostatic potential outside and between the two segments and are used to align the FDR.

Then, anticollinear measurements were performed with different laser frequencies so that the obtained resonance spectra spanned the complete scan-voltage range, and the kinetic beam energy was extracted with Eq. (3). The corresponding laser frequency ν_{lab} was measured with a frequency comb, and the total uncertainty of the extracted effective voltage applied to the detection region was less than 0.05 V. In parallel, the applied scan voltage was measured with a Keysight 3458A 8.5-digit multimeter. As both chambers are designed to efficiently collect fluorescence photons on one or two photomultiplier tubes, only the average field penetration of the chamber can be extracted.

In Fig. 8(a), the laser-based measurement of the total acceleration voltage of the ions is shown relative to the applied and electronically measured voltage for the two chambers of the fluorescence detection region. The first chamber is equipped with an elliptical mirror set that collects the fluorescence light at one focal axis and guides it to the second focal axis outside the vacuum chamber, at which two photomultiplier tubes (PMTs) are located;[36] see Fig. 7 (1). It has an enclosed geometry, i.e., it is only open toward the PMT and has a 13-mm diameter entry and exit port for the laser and ion beam. The entry and exit ports are connected with a 92-mm long and 13-mm wide tube. Contrarily, chamber 2, which is equipped with a lens to focus the light onto the PMT,[37] has a relatively open geometry without metallic shielding on the sides. This explains the significantly larger field penetration of 1.568 (17)% compared to 0.030 (18)% in chamber 1. As different materials are used in the two chambers (Ch1: Miro UV-C foils from ALANOD; Ch2: machined aluminum), different contact voltages exist, causing an offset of almost 0.6 V, which is of the expected order of magnitude. Afterward, the fluorescence detection region was improved by installing metallic meshes (3×3 mm^2 openings thin space with 1 mm wire) at the opening toward the PMTs of chamber 1 and by enclosing the lens region of chamber 2 with the same mesh. The measurement was repeated, now using the $5s^2S_{1/2} \rightarrow 5p^2P_{1/2}$ transition in $^{88}Sr^+$. As shown in Fig. 8(b), the field penetration was strongly reduced to 0.009 (4)% and 0.059 (3)% in chambers 1 and 2, respectively. Deflections of the ion beam caused by the applied high voltage and misaligned electrodes would also lead to shifts in the resonant laser frequency [see Eq. (1)]. This would cause a parabolic

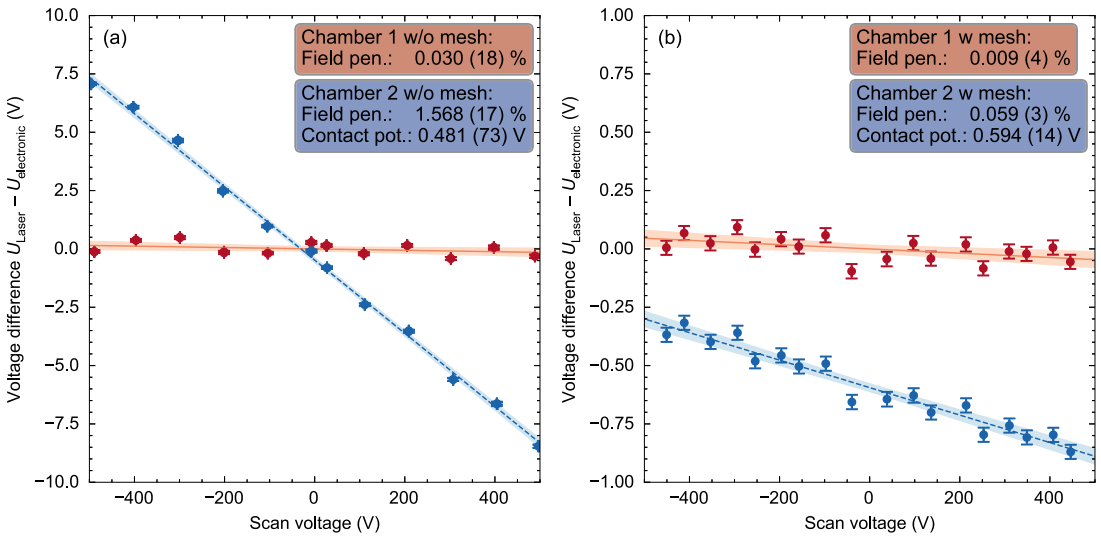

FIG. 8. Difference of the laser spectroscopically determined potential applied to the detection region to an electronic measurement with a multimeter (a) without and (b) with additional shielding by installing a metallic mesh. Without mesh, a large field penetration effect was observed, particularly in chamber 2, which has a more open geometry than chamber 1. Closing the openings with a metallic mesh reduced the field penetration. Between both chambers, a potential offset is observed, which is attributed to contact voltages as different materials are used.

function around 0, which was not observed. Similarly, the wrong gain factor of the multimeter would not cause a linear slope but an inversion at 0. At MSU, the same procedure was applied using the $3p^6 4s^2 S_{1/2} \rightarrow 4p^2 P_{3/2}$ transition (393 nm) in $^{40}Ca^+$, but due to the absence of a frequency comb, a lower resolution was achieved. Here, a field penetration of 0.055 (10)% was observed in the first fluorescence detection chamber,[28] while no field penetration could be resolved for the second chamber. The latter is a copy of the mirror-based chamber at TUDa with mesh. Hence, a penetration of 0.01% is expected. The relative field penetration between the two MSU chambers was confirmed by the measurement of hyperfine spectra in $^{45}Sc^+$ presented in Ref. 38. Generally, the quantification of the field penetration from the measurement of a well-known hyperfine splitting is the easiest approach since such a measurement can be performed at one laser frequency and no frequency comb is required to achieve a high resolution. Reference spectra can be obtained from well-characterized setups, e.g., at TUDa, from precision ion-trap measurements[39–41] or RF atomic beam measurements.[42,43] For example, a measurement of the magnetic hyperfine parameter of the ground state of the stable $^{87}Sr^+$ $A = -1000.473\,673(11)$ MHz[40] in a setup with a field penetration of 0.05% would systematically deviate by 0.5 MHz, shifted to smaller absolute values. An isotope shift measurement of $^{76}Sr^+$ relative to the stable $^{88}Sr^+$ to investigate the impact of the $N = 40$ subshell closure on the charge radius of this $N = Z$ nucleus using a 30-keV ion and pure Doppler tuning would deviate by 25 MHz. Those uncertainties are relevant for state-of-the-art collinear laser spectroscopy experiments as they exceed statistical contributions. As the effect scales linearly, the absolute deviation is smaller for nuclei with small hyperfine splittings and isotopes close to stability. The impact of this systematic deviation on the A parameter on benchmarking atomic calculations, however, is marginal as their precision for multi-electron systems is still limited beyond the MHz level.[44,45] In the extraction of nuclear moments, the systematic contribution cancels as those are determined relative to a reference isotope, which is affected identically. Contrarily, nuclear charge radii are directly affected. However, the trend along the isotopic chain will be correlated, i.e., its slope is systematically tilted, but fine structural details such as the odd–even staggering or kinks at magic numbers, which are especially used to test nuclear theory,[46,47] persist. Charge radius applications that exceed one element, on the other hand, e.g., for the investigation of proton halos,[48] to constrain the slope parameter L of the nuclear equation of state,[49–51] or as input parameters for calculations of CKM matrix elements,[52] are directly afflicted and have to be evaluated carefully.

V. CONCLUSION

The determination of the kinetic beam energy, which is governed by the electrostatic acceleration potential, is crucial for precision fast-beam collinear laser spectroscopy measurements and constitutes the largest systematic uncertainty. The total kinetic beam energy can be extracted from collinear and anticollinear measurements. With new custom-built high-voltage dividers, the acceleration voltage at BECOLA and COALA is precisely measured and stabilized to the ppm level with a feedback loop to eliminate drifts of the kinetic beam energy during the experiment and the corresponding uncertainty contribution. Furthermore, the often neglected impact of field penetration into the optical detection region was investigated, yielding significant contributions if large Doppler tuning voltages are applied. This can be circumvented by performing all measurements at the same scanning voltage, which requires a change in laser frequencies for different isotopes or hyperfine lines. Particularly for the latter, this can become impractical. With quantification of the field penetration into the interaction region, either by performing measurements of the same transition at different scan voltages or easier by measuring a well-known hyperfine splitting, its impact can be attributed in the analysis. The relative uncertainty of such a calibration, here 0.01% and 0.004% for the setups at MSU and TUDa, respectively, is usually below the statistical uncertainty.

ACKNOWLEDGMENTS

We thank Jörg Krämer, Phillip Imgram, and Hendrik Bodnar for their contributions to the experimental developments at COALA, and Uwe Bonnes for designing the custom DAC. We acknowledge the funding by the Deutsche Forschungsgemeinschaft (DFG) Project No. 279384907 SFB 1245, as well as under Grant Nos. INST No. 163/392-1 FUGG and 789/4-1. Furthermore, support was granted from the German Federal Ministry for Education and Research (BMBF) under Contract Nos. 05P21RDFN1 and 05P21RDCI1 and the National Science Foundation under Grant No. PHY-21-11185.

AUTHOR DECLARATIONS

Conflict of Interest

The authors have no conflicts to disclose.

Author Contributions

Kristian König: Conceptualization (lead); Data curation (lead); Formal analysis (lead); Investigation (lead); Methodology (lead); Project administration (lead); Software (equal); Supervision (lead); Validation (lead); Visualization (lead); Writing – original draft (lead). **Finn Köhler**: Data curation (equal); Formal analysis (equal); Investigation (equal); Software (equal); Writing – original draft (equal). **Julian Palmes**: Data curation (equal); Formal analysis (equal); Investigation (equal); Writing – original draft (equal). **Henrik Badura**: Data curation (equal). **Adam Dockery**: Data curation (equal); Investigation (equal). **Kei Minamisono**: Conceptualization (equal); Funding acquisition (equal); Project administration (equal); Resources (equal); Supervision (equal); Writing – review & editing (equal). **Johann Meisner**: Methodology (equal); Resources (equal); Writing – review & editing (equal). **Patrick Müller**: Conceptualization (equal); Investigation (equal); Software (equal); Writing – review & editing (equal). **Wilfried Nörtershäuser**: Funding acquisition (equal); Project administration (equal); Resources (equal); Writing – review & editing (equal). **Stephan Passon**: Conceptualization (equal); Methodology (equal); Writing – review & editing (equal).

DATA AVAILABILITY

The data that support the findings of this study are available from the corresponding author upon reasonable request.

REFERENCES

[1] M. Aker, A. Beglarian, J. Behrens *et al.*, Nat. Phys. **18**, 160 (2022).
[2] M. Arenz, W.-J. Baek, M. Beck, A. Beglarian, J. Behrens, T. Bergmann, A. Berlev, U. Besserer, K. Blaum, T. Bode, B. Bornschein, L. Bornschein, T. Brunst, N. Buzinsky, S. Chilingaryan, W. Choi, M. Deffert, P. Doe, O. Dragoun, G. Drexlin *et al.*, Eur. Phys. J. C **78**, 368 (2018).
[3] A. Bartoloni, L. Barone, F. Cavallari, I. Dafinei, D. del Re, M. Diemoz, S. Guerra, E. Longo, P. Meridiani, G. Organtini, A. Palma, R. Paramatti, F. Pellegrino, S. Rahatlou, C. Rovelli, and F. Santanastasio, Nucl. Instrum. Methods Phys. Res., Sect. A **582**, 462 (2007).
[4] C. Böhm, S. Sturm, A. Rischka, A. Dörr, S. Eliseev, M. Goncharov, M. Höcker, J. Ketter, F. Köhler, D. Marschall, J. Martin, D. Obieglo, J. Repp, C. Roux, R. Schüssler, M. Steigleder, S. Streubel, T. Wagner, J. Westermann, V. Wieder, R. Zirpel, J. Melcher, and K. Blaum, Nucl. Instrum. Methods Phys. Res., Sect. A **828**, 125 (2016).
[5] F. Wienholtz, K. Blaum, J. Karthein, D. Lunney, S. Malbrunot-Ettenauer, V. Manea, M. Mougeot, L. Schweikhard, T. Steinsberger, and R. Wolf, Nucl. Instrum. Methods Phys. Res., Sect. B **463**, 348 (2020).
[6] M. Cavenago, C. Baltador, L. Bellan, M. Comunian, A. De Lorenzi, E. Fagotti, A. Galatà, A. Palmieri, A. Pisent, and M. Rossignoli, in *2020 29th International Symposium on Discharges and Electrical Insulation in Vacuum (ISDEIV)* (IEEE, 2021), pp. 426–429.
[7] A. Krieger, C. Geppert, R. Catherall, F. Hochschulz, J. Krämer, R. Neugart, S. Rosendahl, J. Schipper, E. Siesling, C. Weinheimer, D. Yordanov, and W. Nörtershäuser, Nucl. Instrum. Methods Phys. Res., Sect. A **632**, 23 (2011).
[8] J. Ullmann, Z. Andelkovic, C. Brandau, A. Dax, W. Geithner, C. Geppert, C. Gorges, M. Hammen, V. Hannen, S. Kaufmann, K. König, Y. Litvinov, M. Lochmann, B. Maaß, J. Meisner, T. Murböck, R. Sánchez, M. Schmidt, S. Schmidt, M. Steck *et al.*, Nat. Commun. **8**, 15484 (2017).
[9] K. Yan, Y. Zhou, X. Ma, M. Tang, D. Gao, H. Zhao, Z. Huang, W. Wen, and L. Mao, Nucl. Instrum. Methods Phys. Res., Sect. A **1046**, 167699 (2023).
[10] M. Bishof, R. H. Parker, K. G. Bailey, J. P. Greene, R. J. Holt, M. R. Kalita, W. Korsch, N. D. Lemke, Z.-T. Lu, P. Mueller, T. P. O'Connor, J. T. Singh, and M. R. Dietrich, Phys. Rev. C **94**, 025501 (2016).
[11] M. Lochmann, R. Jöhren, C. Geppert, Z. Andelkovic, D. Anielski, B. Botermann, M. Bussmann, A. Dax, N. Frömmgen, M. Hammen, V. Hannen, T. Kühl, Y. A. Litvinov, R. López-Coto, T. Stöhlker, R. C. Thompson, J. Vollbrecht, A. Volotka, C. Weinheimer, W. Wen, E. Will, D. Winters, R. Sánchez, and W. Nörtershäuser, Phys. Rev. A **90**, 030501 (2014).
[12] P. Campbell, I. Moore, and M. Pearson, "Laser spectroscopy for nuclear structure physics," Prog. Part. Nucl. Phys. **86**, 127 (2016).
[13] X. Yang, S. Wang, S. Wilkins, and R. G. Ruiz, "Laser spectroscopy for the study of exotic nuclei," Prog. Part. Nucl. Phys. **129**, 104005 (2023).
[14] M. Verlinde, K. Dockx, S. Geldhof, K. König, D. Studer, T. E. Cocolios, R. P. de Groote, R. Ferrer, Y. Kudryavtsev, T. Kieck, I. Moore, W. Nörtershäuser, S. Raeder, P. van den Bergh, P. van Duppen, and K. Wendt, Appl. Phys. B **126**, 85 (2020).
[15] K. König, P. Imgram, J. Krämer, B. Maaß, K. Mohr, T. Ratajczyk, F. Sommer, and W. Nörtershäuser, Appl. Phys. B **126**, 86 (2020).
[16] K. König, K. Minamisono, J. Lantis, S. Pineda, and R. Powel, Phys. Rev. A **103**, 032806 (2021).
[17] W. D. Chen, J. Xiao, Y. Shen, Y. Q. Fu, F. C. Meng, C. Y. Chen, Y. Zou, and R. Hutton, Rev. Sci. Instrum. **79**, 123304 (2008).
[18] T. Thümmler, R. Marx, and C. Weinheimer, New J. Phys. **11**, 103007 (2009).
[19] P. Schury, M. Wada, H. Wollnik, J.-Y. Moon, T. Hashimoto, and M. Rosenbusch, Rev. Sci. Instrum. **91**, 014702 (2020).
[20] P. Fischer and L. Schweikhard, Rev. Sci. Instrum. **92**, 063203 (2021).
[21] M. Miwa, S. Matsuyama, and S. Toyama, Nucl. Instrum. Methods Phys. Res., Sect. B **543**, 165101 (2023).
[22] W. Geithner, T. Neff, G. Audi, K. Blaum, P. Delahaye, H. Feldmeier, S. George, C. Guenaut, F. Herfurth, A. Herlert, S. Kappertz, M. Keim, A. Kellerbauer, H. J. Kluge, M. Kowalska, P. Lievens, D. Lunney, K. Marinova, R. Neugart, L. Schweikhard, S. Wilbert, and C. Yazidjian, Phys. Rev. Lett. **101**, 252502 (2008).
[23] W. Nörtershäuser, D. Tiedemann, M. Zakova, Z. Andjelkovic, K. Blaum, M. L. Bissell, R. Cazan, G. W. F. Drake, C. Geppert, M. Kowalska, J. Krämer, A. Krieger, R. Neugart, R. Sanchez, F. Schmidt-Kaler, Z. C. Yan, D. T. Yordanov, and C. Zimmermann, Phys. Rev. Lett. **102**, 062503 (2009).
[24] E. Riis, H. G. Berry, O. Poulsen, S. A. Lee, and S. Y. Tang, Phys. Rev. A **33**, 3023 (1986).
[25] A. Krieger, K. Blaum, M. L. Bissell, N. Frömmgen, C. Geppert, M. Hammen, K. Kreim, M. Kowalska, J. Krämer, T. Neff, R. Neugart, G. Neyens, W. Nörtershäuser, C. Novotny, R. Sanchez, and D. T. Yordanov, Phys. Rev. Lett. **108**, 142501 (2012).
[26] S. Götte, K.-M. Knaak, N. Kotovski, H.-J. Kluge, G. Ewald, and K. D. A. Wendt, Rev. Sci. Instrum. **75**, 1039 (2004).
[27] J. Krämer, K. König, G. Ch, P. Imgram, B. Maaß, J. Meisner, E. W. Otten, S. Passon, T. Ratajczyk, J. Ullmann, and W. Nörtershäuser, Metrologia **55**, 268 (2018).
[28] K. Minamisono, P. Mantica, A. Klose, S. Vinnikova, A. Schneider, B. Johnson, and B. Barquest, Nucl. Instrum. Methods Phys. Res., Sect. A **709**, 85 (2013).
[29] K. König, J. Krämer, C. Geppert, P. Imgram, B. Maaß, T. Ratajczyk, and W. Nörtershäuser, Rev. Sci. Instrum. **91**, 081301 (2020).
[30] P. Müller, K. König, P. Imgram, J. Krämer, and W. Nörtershäuser, Phys. Rev. Res. **2**, 043351 (2020).
[31] P. Imgram, K. König, B. Maaß, P. Müller, and W. Nörtershäuser, Phys. Rev. A **108**, 062809 (2023).
[32] P. Imgram, K. König, B. Maaß, P. Müller, and W. Nörtershäuser, Phys. Rev. Lett. **131**, 243001 (2023).
[33] S. Passon, K. König, F. Schilling, B. Maaß, J. Meisner, and W. Nörtershäuser, "Ultra-stable 3d-printed precision voltage divider for calibrations and experiments," arXiv:2407.06700 [physics.ins-det] (2024).
[34] R. Marx, IEEE Trans. Instrum. Meas. **50**, 426 (2001).
[35] J. Berengut *et al.*, Phys. Rev. Lett. **120**, 091801 (2018).
[36] B. Maaß, K. König, J. Krämer, A. Miller, K. Minamisono, W. Nörtershäuser, and F. Sommer, "A 4π fluorescence detection region for collinear laser spectroscopy," arXiv:2007.02658 [physics.ins-det] (2020).
[37] P. Müller, "Laserspectroscopic determination of the nuclear charge radius of ^{13}C," Ph.D. thesis, Technische Universität, Darmstadt, 2024.
[38] A. Dockery, K. König, J. Lantis, Y. Liu, K. Minamisono, S. Pineda, and R. Powel, Phys. Rev. A **108**, 052816 (2023).
[39] W. M. Itano and D. J. Wineland, Phys. Rev. A **24**, 1364 (1981).
[40] H. Sunaoshi, Y. Fukashiro, M. Furukawa, M. Yamauchi, S. Hayashibe, T. Shinozuka, M. Fujioka, I. Satoh, M. Wada, and S. Matsuki, Hyperfine Interact. **78**, 241 (1993).
[41] F. Arbes, M. Benzing, T. Gudjons, F. Kurth, and G. Werth, Z. Phys. D At., Mol. Clusters **31**, 27 (1994).
[42] W. J. Childs and L. S. Goodman, Phys. Rev. A **20**, 1922 (1979).
[43] W. J. Childs and L. S. Goodman, Phys. Rev. A **24**, 1342 (1981).
[44] B. Lu, X. Lu, T. Wang, and H. Chang, J. Phys. B: At., Mol. Opt. Phys. **55**, 205002 (2022).
[45] M. Ma, Y. Li, M. Godefroid, G. Gaigalas, J. Li, J. Bieroń, C. Chen, J. Wang, and P. Jönsson, Atoms **12**, 30 (2024).
[46] R. de Groote, J. Billowes, C. Binnersley, M. Bissell, T. Cocolios, T. Day-Goodacre, G. Farooq-Smith, D. Fedorov, K. Flanagan, S. Franchoo, R. Garcia-Ruiz, W. Gins, J. Holt, A. Koszorus, K. Lynch, T. Miyagi, W. Nazarewicz, G. Neyens, P. Reinhard, S. Rothe *et al.*, Nat. Phys. **16**, 620 (2020).
[47] A. Koszorus, X. Yang, W. Jiang, S. Novario, S. Bai, J. Billowes, C. Binnersley, M. Bissell, T. Cocolios, B. Cooper, R. de Groote, A. Ekström, K. Flanagan, C. Forssén, S. Franchoo, R. Garcia Ruiz, F. Gustafsson, G. Hagen, G. Jansen, and S. Wilkins, Nat. Phys. **17**, 439 (2021).
[48] B. Maaß, P. Müller, W. Nörtershäuser, J. Clark, C. Gorges, S. Kaufmann, K. König, J. Krämer, A. Levand, R. Orford, R. Sánchez, G. Savard, and F. Sommer, Hyperfine Interact. **238**, 25 (2017).
[49] B. A. Brown, Phys. Rev. Lett. **119**, 122502 (2017).
[50] B. A. Brown, K. Minamisono, J. Piekarewicz, H. Hergert, D. Garand, A. Klose, K. König, J. D. Lantis, Y. Liu, B. Maaß, A. J. Miller, W. Nörtershäuser, S. V. Pineda, R. C. Powel, D. M. Rossi, F. Sommer, C. Sumithrarachchi, A. Teigelhöfer, J. Watkins, and R. Wirth, Phys. Rev. Research **2**, 022035 (2020).
[51] S. V. Pineda, K. König, D. M. Rossi, B. A. Brown, A. Incorvati, J. Lantis, K. Minamisono, W. Nörtershäuser, J. Piekarewicz, R. Powel, and F. Sommer, Phys. Rev. Lett. **127**, 182503 (2021).

[52]P. Plattner, E. Wood, L. Al Ayoubi, O. Beliuskina, M. L. Bissell, K. Blaum, P. Campbell, B. Cheal, R. P. de Groote, C. S. Devlin, T. Eronen, L. Filippin, R. F. Garcia Ruiz, Z. Ge, S. Geldhof, W. Gins, M. Godefroid, H. Heylen, M. Hukkanen, P. Imgram, A. Jaries, A. Jokinen, A. Kanellakopoulos, A. Kankainen, S. Kaufmann, K. König, A. Koszorús, S. Kujanpää, S. Lechner, S. Malbrunot-Ettenauer, P. Müller, R. Mathieson, I. Moore, W. Nörtershäuser, D. Nesterenko, R. Neugart, G. Neyens, A. Ortiz-Cortes, H. Penttilä, I. Pohjalainen, A. Raggio, M. Reponen, S. Rinta-Antila, L. V. Rodríguez, J. Romero, R. Sánchez, F. Sommer, M. Stryjczyk, V. Virtanen, L. Xie, Z. Y. Xu, X. F. Yang, and D. T. Yordanov, Phys. Rev. Lett. **131**, 222502 (2023).